

**$T_d$  to  $1T'$  structural phase transition in the  $WTe_2$  Weyl semimetal**Yu Tao<sup>1</sup>,<sup>\*</sup> John A. Schneeloch<sup>1</sup>, Adam A. Aczel<sup>2,3</sup> and Despina Louca<sup>1,\*</sup><sup>1</sup>*Department of Physics, University of Virginia, Charlottesville, Virginia 22904, USA*<sup>2</sup>*Neutron Scattering Division, Oak Ridge National Laboratory, Oak Ridge, Tennessee 37831, USA*<sup>3</sup>*Department of Physics and Astronomy, University of Tennessee, Knoxville, Tennessee 37996, USA*

(Received 23 March 2020; revised 10 June 2020; accepted 30 July 2020; published 24 August 2020)

Elastic neutron scattering on a single crystal combined with powder x-ray diffraction measurements were carried out to investigate how the crystal structure evolves as a function of temperature in the Weyl semimetal  $WTe_2$ . A sharp transition from the low-temperature orthorhombic phase ( $T_d$ ) to the high-temperature monoclinic phase ( $1T'$ ) was observed at ambient pressure in the single crystal near  $\sim 565$  K. Unlike in  $MoTe_2$ , the solid-solid transition from  $T_d$  to  $1T'$  occurs without the cell doubling of the intermediate  $T_d^*$  phase with AABB (or ABBA) layer stacking. In powders, however, the thermal transition from the  $T_d$  to the  $1T'$  phase was broadened and a two-phase coexistence was observed until 700 K, well above the structural transition.

DOI: [10.1103/PhysRevB.102.060103](https://doi.org/10.1103/PhysRevB.102.060103)**I. INTRODUCTION**

Transition metal dichalcogenides have attracted considerable attention recently because of their intriguing electronic band structure properties that render them hosts to exotic quasiparticles.  $MoTe_2$  and  $WTe_2$  are reported to be type-II Weyl semimetals in the orthorhombic  $T_d$  phase [1,2] due to inversion symmetry breaking, and both show a large nonsaturating magnetoresistance [3–5]. They are layered structures, held together by van der Waals forces, and can undergo multiple solid-solid transitions through the sliding of layers [6,7]. Upon quenching from high temperatures, the monoclinic phase,  $1T'$ , was first shown to be stabilized in  $MoTe_2$ , from which the low-temperature orthorhombic phase ( $T_d$ ) emerges. The high-temperature monoclinic phase [6] and the low-temperature orthorhombic phase differ in their layer stacking. In  $WTe_2$ , on the other hand, only the  $T_d$  phase has been reported at ambient pressure, and the  $1T'$  phase has been theoretically predicted to be absent up to at least 500 K [8]. Application of external pressure, however, leads to a  $T_d$  to  $1T'$  phase transition that commences around 6.0 GPa [9].

The  $1T'$  crystal structure is shown in Fig. 1(a), projected in the  $a$ - $c$  plane. Layer stacking follows two possible ordering schemes, with stacking types labeled “A” and “B” [Fig. 1(b)] [10,11]. The  $T_d$  phase is constructed by stacking either AAAA... or BBBB... sequences, while the  $1T'$  is built by stacking ABAB... or BABA... layers. We recently reported that an intermediate pseudo-orthorhombic  $T_d^*$  phase appears across the transition boundary between  $T_d$  and  $1T'$ , with an AABB... (or ABBA...) layer stacking in  $MoTe_2$ . The  $T_d^*$  phase is only observed upon warming, while on cooling, diffuse scattering is seen, most likely arising from a frustrated tendency towards the  $T_d^*$  stacking order [11,12]. Regardless of A- or B-type stacking, all pairs of neighboring layers are

positioned relative to each other in essentially the same way, which can be captured by an in-plane displacement parameter  $\delta$  [13], as shown in Fig. 1(a). We define  $\delta$  as the distance along the  $a$  axis between the midpoints of metal-metal bonds of neighboring layers; this definition is uniquely defined for both  $1T'$  (where it is related to the  $\beta$  angle) and  $T_d$ .

With W substitution as in  $Mo_{1-x}W_xTe_2$ , the  $1T'$  to  $T_d$  structural transition temperature increases up until  $x \approx 0.57$  [14]. However, it is not known at present whether this transition occurs at ambient pressure at the other end of the phase diagram with  $x = 1$  as in  $WTe_2$ . A pressure-driven  $T_d$ - $1T'$  structural transition has been reported to appear at 4–5 GPa [15], at 8 GPa [16], and in a broad range from 6.0 to 18.2 GPa, during which a volume collapse with dramatic changes in the lattice constants was observed [9]. In  $MoTe_2$ , pressure suppresses the temperature of the  $1T'$ - $T_d$  transition, and extinguishes it by  $\sim 1.2$  GPa [12,17,18], though dramatic changes in the lattice constants between the phases have not been reported. Nonetheless, the presence of a transition in  $WTe_2$  under pressure, as well as the trend of increasing  $T_d$ - $1T'$  transition temperature with W substitution in the  $Mo_{1-x}W_xTe_2$  [14,19–21] phase diagram suggest the possibility of an ambient-pressure transition at high temperatures.

Using elastic neutron scattering, we observed the  $T_d$ - $1T'$  structural phase transition at ambient pressure in a single crystal of  $WTe_2$ . The transition is sharp, occurs at  $\sim 565$  K, and proceeds without hysteresis. No intermediate phase is present across the phase boundary in  $WTe_2$ , in contrast to the  $T_d^*$  phase seen in  $MoTe_2$ . From powder x-ray diffraction (XRD), however, the transition appears broad and incomplete up to 700 K, with phase coexistence across a wide temperature range.

**II. EXPERIMENTAL DETAILS**

The  $WTe_2$  single crystals were grown out of a Te flux. First,  $WTe_2$  powder was prepared from stoichiometric ratios

\*Corresponding author: [louca@virginia.edu](mailto:louca@virginia.edu)

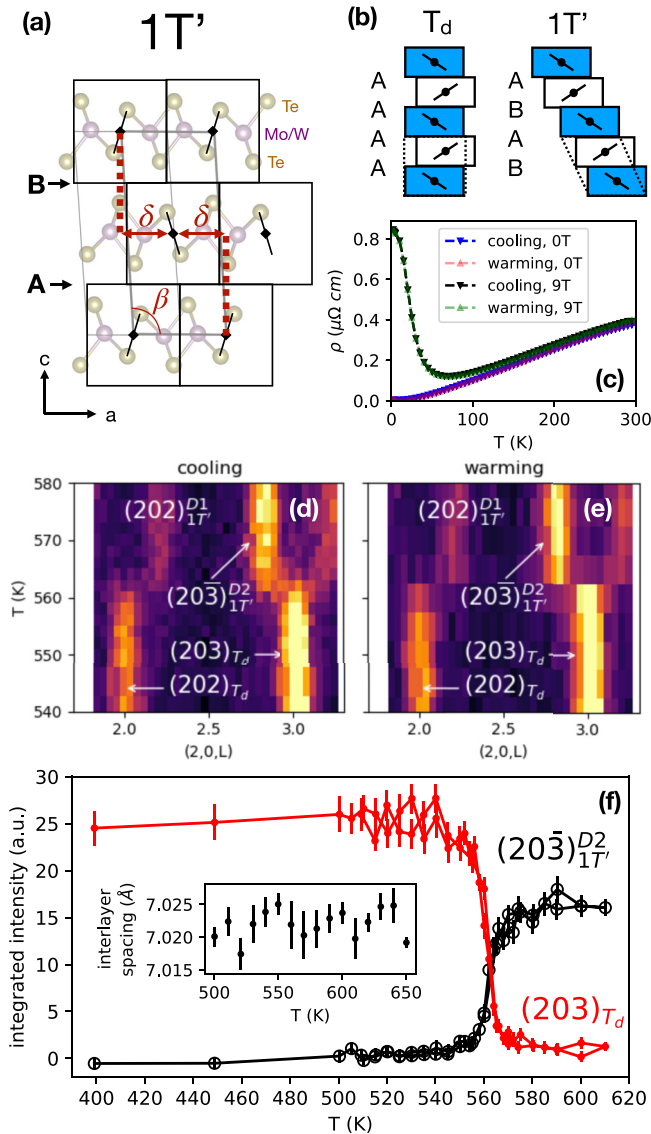


FIG. 1. (a) The crystal structure of  $1T'$ - $\text{Mo}_{1-x}\text{W}_x\text{Te}_2$  projected in the  $a$ - $c$  plane. (b) Stacking sequences for the  $T_d$  and  $1T'$  phases of  $\text{WTe}_2$ . (c) Temperature and field dependence of resistivity in  $\text{WTe}_2$ , for current along the  $b$  direction and  $H \parallel c$ . The relative error of each data point is  $\sim 0.001$ . (d), (e) Scans of neutron scattering intensity along  $(2, 0, L)$  collected on a single crystal of  $\text{WTe}_2$  on cooling and warming. The Bragg peaks labeled  $D1$  and  $D2$  refer to the two  $1T'$  twins. (f) Intensity as a function of temperature of  $(203)_{T_d}$  and  $(20\bar{3})_{1T'}$ , obtained from fits of scans along  $(2, 0, L)$ . [inset of (f)] The temperature dependence of the interlayer spacing, obtained from fits to longitudinal scans along  $(004)$ .

of W and Te powders. The sintering was done in an evacuated quartz silica ampoule at  $900^\circ\text{C}$  for 2 days. The sintered powder was then pressed into a pellet and sealed with excess Te in a molar ratio of 1:13. The ampoule was placed horizontally in a tube furnace and heated at a constant temperature of  $850^\circ\text{C}$  for 7 days. Excess Te was removed by reinserting one end of the ampoule into a tube furnace at  $\sim 900^\circ\text{C}$  and decanting the molten Te towards the cold end. For powder XRD, powder was sintered as described above.

Resistivity measurements under magnetic fields of 0 and 9 T are shown in Fig. 1(c). The residual resistivity ratio (RRR) from the 0 T data is calculated to be  $\sim 118(3)$ . Our  $\text{WTe}_2$  crystals also have a large magnetoresistance, with a magnitude of 51 553% at 2 K under a 9 T magnetic field. These values are reasonably high [22], though higher values have been reported in the literature, such as an RRR of  $\sim 370$  and a magnetoresistance of 452 700% at 4.5 K in an applied field of 14.7 T [4].

Elastic neutron scattering was performed on the triple axis spectrometer HB1A, located at the High Flux Isotope Reactor at Oak Ridge National Laboratory. The elastic measurements used an incident neutron energy of 14.6 meV and the collimation was  $40'-40'\text{-S-}40'\text{-}80'$ . The crystal was mounted to an aluminum plate via aluminum wire, and a furnace was used to control the temperature. Powder XRD measurements were collected on a laboratory x-ray diffractometer (Rigaku Smartlab SE with an Anton-Paar TTK600 unit) as a function of temperature between 300 and 700 K. Rietveld refinement was done using the GSAS-II software [23]. In this Rapid Communication, we use atomic coordinates based on an orthorhombic unit cell with  $b < a < c$  (i.e.,  $a \approx 6.28 \text{ \AA}$ ,  $b \approx 3.496 \text{ \AA}$ , and  $c \approx 14.07 \text{ \AA}$ ).

### III. RESULTS AND DISCUSSION

Shown in Figs. 1(d) and 1(e) are intensity maps which combine elastic neutron scattering scans along  $(2, 0, L)$  at a sequence of temperatures on warming from 510 to 610 K, then cooling. A clear  $T_d$ - $1T'$  transition can be seen from changes in the Bragg peaks, which occur without the diffuse scattering seen in  $\text{MoTe}_2$  [11]. At low temperatures, the  $(202)_{T_d}$  and  $(20\bar{3})_{T_d}$  Bragg peaks are observed. On warming, a structural phase transition into the  $1T'$  phase is observed at  $\sim 565$  K, followed by  $1T'$  phase peaks appearing near  $L \approx 2.2$  and 2.8. The calculated volume fractions of the  $1T'$  twins are around 48% and 52%. Unlike the appearance of the  $T_d^*$  phase in  $\text{MoTe}_2$ , there is no intermediate phase present in the transition in  $\text{WTe}_2$ .

In Fig. 1(f), the intensities of the  $(203)_{T_d}$  and  $(20\bar{3})_{1T'}$  peaks, obtained from fits to scans along  $(2, 0, L)$ , are plotted as a function of temperature on warming and cooling through the hysteresis loop. The transition in  $\text{WTe}_2$  is quite sharp (mostly complete within  $\sim 10$  K) with very little hysteresis, as seen from the overlap of the warming and cooling curves. In contrast,  $\text{MoTe}_2$  has a broader transition of tens of kelvins, with a lingering hysteresis in the resistivity that can persist hundreds of kelvins away from the transition region [11]. Although structural phase transitions are often accompanied by anomalies in the lattice constants, no change in the interlayer spacing was observed in the inset of Fig. 1(f), in contrast to the abrupt changes seen under pressure for the lattice constants [9]. The  $a$  axis did not change dramatically either, given the similar intensities of  $(2, 0, L)$  scans which were performed across the transition without realignment.

In contrast to the clean transition seen in the single crystal, we observe a broad  $T_d$ - $1T'$  transition in powder  $\text{WTe}_2$  on warming to 700 K. XRD patterns at 300 and 700 K are shown in Figs. 2(a) and 2(b). (Data for other temperatures are shown in the Supplemental Material [24].) At 300 K, peaks from

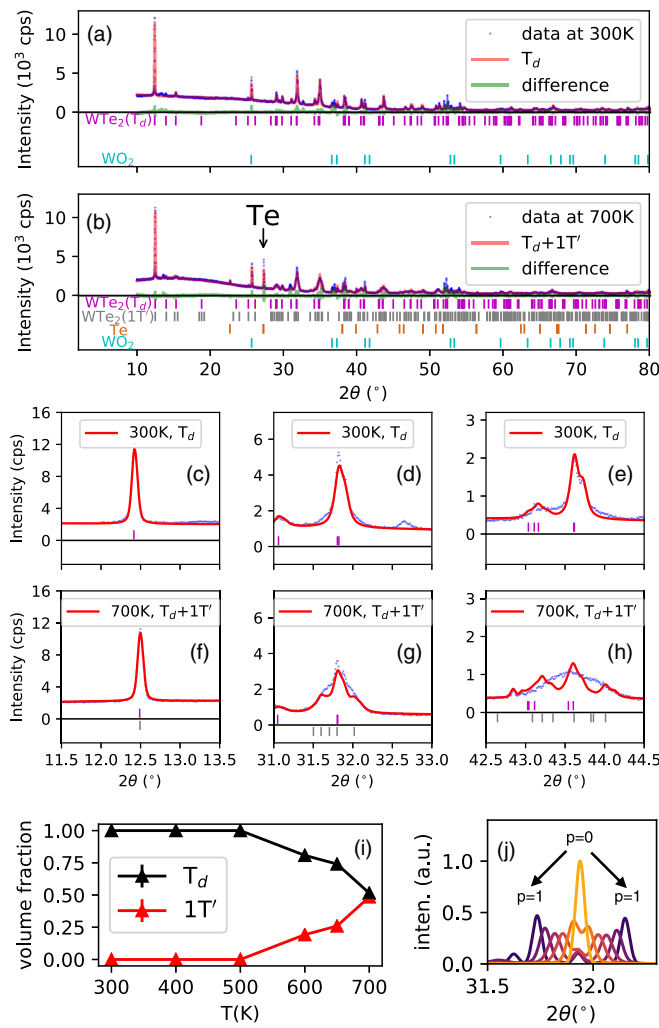


FIG. 2. (a), (b) A plot of the x-ray diffraction pattern compared to the refined model for the average symmetry of powder  $WTe_2$ , collected at 300 and 700 K on warming. Pure Te Bragg peaks are observed at 700 K. (c)–(h) Diffraction data plotted in a narrow range (blue dashed lines) for 300 K (c)–(e) and 700 K (f)–(h) for the (0, 0, 2) peak (c), (f) and two other peaks. The red curves correspond to the calculated intensity for the  $T_d$  phase or a  $T_d$ - $1T'$  phase coexistence, respectively. (i) The volume fractions of the  $T_d$  and  $1T'$  phases as a function of temperature. (j) Simulated XRD intensities for  $T_d$  ( $p = 0$ ),  $1T'$  ( $p = 1$ ), and disordered stacking ( $0 < p < 1$ ), intermediate between  $T_d$  and  $1T'$ , for the same regions as (d) and (g).  $p$  is the probability of a random swap of “A” with “B”-type stacking for every other interlayer boundary in the  $T_d$  AAAA... stacking.

the  $T_d$  phase can be seen, as well as an impurity  $WO_2$  phase having weight percent 5.1(1)%. At 700 K, the pattern can be better fit by a combination of  $T_d$  and  $1T'$ , as depicted in Figs. 2(c)–2(h). The  $WO_2$  impurity phase was still present at 700 K. Peaks belonging to Te arose, first observable around 600 K, and reaching a weight percent of 8.13(17)% by 700 K. These Te peaks suggest the decomposition of  $WTe_2$ , though refinement suggested no Te vacancies; a refinement of 700 K data with the occupancies of all Te atoms in  $T_d$ - and  $1T'$ - $WTe_2$  fixed to a single value yielded a composition of  $WTe_{2.016(18)}$ .

Though decomposition implies that elemental W should be present, no W peaks were seen. The relative volume fractions for the  $1T'$  and  $T_d$  contributions are shown in Fig. 2(i). The transition in the  $WTe_2$  powder is much broader than in the single crystal, beginning between 500 and 600 K, and steadily increasing up to at least 700 K.

At 700 K, comparing the data with a model for a mixture of  $T_d$  and  $1T'$  phases [Figs. 2(g) and 2(h)] shows that the changes in intensity roughly correspond to that expected from  $1T'$ . (The  $\beta$  angle for  $1T'$  was set to be consistent with the  $\delta$  parameter derived from the coordinates of the  $T_d$ -phase portion at 700 K.) However, the model produces an intensity curve with distinct peaks, in contrast to the broader distribution seen in the XRD data [e.g., in Fig. 2(h)]. If the broadening were due to a decomposition-induced spread in lattice constants, we might expect the (00L) peaks to also be broadened, while little changes in the (00L) peaks would be expected from disordered stacking since the (00L) peak intensities only depend on atomic position along the out-of-plane axis. Indeed, we see a lack of broadening of the (002) peak between Figs. 2(c) and 2(f), suggesting that the broadness in Figs. 2(g) and 2(h) is due to disordered stacking.

To illustrate how disordered stacking could account for the broadness of many of the XRD peaks at 700 K, we show simulated XRD patterns from disordered stacking sequences progressing from  $T_d$  to  $1T'$  in Fig. 2(j). While a variety of disordered stackings are conceivable, we used a simple stacking model starting from the AAAA... stacking of the  $T_d$  phase, then swapping “A” with “B”-type stacking with probability  $p$  for every other interlayer boundary [10]. Thus,  $p = 0$  and  $p = 1$  correspond to  $T_d$  and  $1T'$ , respectively. The diffuse scattering was obtained from the structure factor of the Bragg peaks of a constructed 1000-layer supercell. Increasing  $p$  from 0 results in a steady shift of intensity toward the locations of the  $1T'$  peaks. Though the intensity shows distinct peaks, even for intermediate  $p$ , a broader intensity distribution could result from inhomogeneity in the values of  $p$ , or from a more complex model of stacking disorder.

An essential parameter that characterizes in-plane positioning of neighboring layers of the  $Mo_{1-x}W_xTe_2$  structure is the  $\delta$  parameter. From the refined coordinates of the  $T_d$  phase XRD data, we obtained  $\delta$  as a function of temperature [Fig. 3(a)]. The  $\delta$  parameter decreases by  $\sim 0.007$  from 300 to 600 K, which is very similar to the decrease in  $Mo_{0.91}W_{0.09}Te_2$  ( $\sim 0.006$  from 320 to 600 K). For the  $1T'$  phase in the single crystal, we can obtain  $\delta$  from the separation between opposite-twin  $1T'$  peaks, yielding 0.5482(3) at 610 K [and a monoclinic  $\beta$  angle of  $92.456(17)^\circ$ ]. This latter value is probably more reliable than those from powder refinement, which may be more insidiously affected by systematic errors due to the indirect nature of obtaining positions from Bragg peak intensities. Nevertheless, a rough agreement for  $\delta$  is found between values obtained from  $T_d$ -phase powder refinement and from the  $1T'$  peak splitting in the single crystal, as seen in Fig. 3(a). The refined  $T_d$ -phase lattice parameters are shown in Figs. 3(b)–3(d). Aside from a possible anomaly near 700 K, which may be related to the decomposition that results in the Te phase, or to the difficulty in refining with stacking disorder present, we see the expected thermal expansion for  $a$ ,  $b$ , and  $c$ .

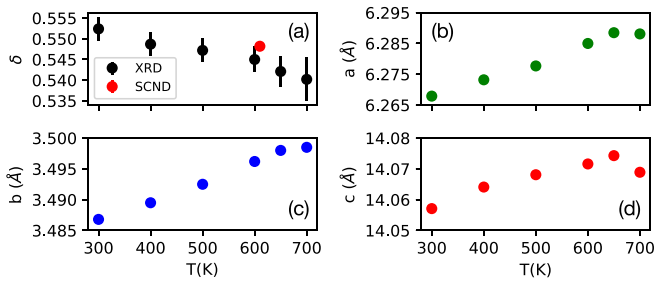


FIG. 3. (a) The temperature dependence of the  $\delta$  parameter of  $\text{WTe}_2$  from powder XRD (black) and single crystal neutron diffraction (SCND) (red) measured on HB1A. (b)–(d) The temperature dependence of the lattice constants  $a$ ,  $b$ , and  $c$ . The error bars for the points in (a)–(d) are smaller than the symbols except for the XRD  $\delta$  points in (a).

Our finding of a  $T_d$ - $1T'$  structural phase transition in  $\text{WTe}_2$  suggests that theories of the transition be revisited. Although the relative stability of  $1T'$  over  $T_d$  in  $\text{MoTe}_2$  at higher temperature has been supported by density functional theory calculations [8,18],  $\text{WTe}_2$  is predicted not to have a transition up to 500 K, and likely much higher [8]. In  $\text{MoTe}_2$ , the preference for  $1T'$  at high temperature is attributed to the phonon entropy contribution (with a lack of soft mode behavior noted) [18], and more accurate calculations (possibly with anharmonicity accounted for as in Ref. [18]) may suggest a similar reason for the existence of  $1T'$  in  $\text{WTe}_2$ . However, there are two theoretical obstacles. First, there is the inherent difficulty in calculating the very small free-energy differences between structures which differ only in the stacking of weakly interacting layers. Second, beyond the relative stability of  $1T'$  and  $T_d$ , to our knowledge, no theoretical attempts have been made to explain the details of the transition, including the existence/absence of a hysteresis, presence of  $T_d^*$  on warming, stacking disorder in other parts of the transition, gradual disappearance of stacking disorder on warming/cooling away from the transition, etc. [11]. Interestingly, the calculations in Ref. [8] show a lack of an energy barrier in  $\text{WTe}_2$  between  $1T'$  and  $T_d$ , in contrast to  $\text{MoTe}_2$ , which may be related to the lack of hysteresis in  $\text{WTe}_2$  but not in  $\text{MoTe}_2$ . However, other factors, such as the increased thermal energy at higher temperature facilitating layer movement, may play a role as well.

The structural trends shown in our data place constraints on theoretical models for the transition. We observed no detectable change in the interlayer spacing across the transition, similar to the negligible change seen in other  $\text{Mo}_{1-x}\text{W}_x\text{Te}_2$  crystals [13]. The lack of an abrupt change in layer spacing highlights the similarities between the phases. Such similarities may make sufficiently accurate calculations difficult, with subtle effects such as spin-orbit coupling contributing non-negligibly to the layer spacing [8]. Meanwhile, theory already appears to be consistent with the decrease in  $\delta$  with W substitution, with calculated values of  $\delta = 0.540$  for  $\text{WTe}_2$  vs  $\delta = 0.564$  for  $\text{MoTe}_2$  (as extracted from calculated  $1T'$  lattice constants), and experimental values of 0.552 for our powder  $T_d$ - $\text{WTe}_2$  data vs 0.574 reported for  $1T'$ - $\text{MoTe}_2$  [18] (both at 300 K).

There are several reasons why the transition may be broader in  $\text{WTe}_2$  powder than in single crystals. First, Te vacancies may be responsible, as they have been proposed to broaden the transition in  $\text{MoTe}_{2-z}$  crystals [25]. Though refinement of our XRD powder data showed no Te vacancies, the presence of stacking disorder increases the difficulty of accurately determining parameters such as the occupancy of atomic sites. A second possibility is that the transition is broadened due to the smallness of the crystallites in a powder. In thin  $\text{MoTe}_2$  crystals (hundreds of nanometers or less) the transition is known to be broadened or suppressed completely [26–28]. Third, there are likely more defects in powder, induced during sintering or grinding. Defects may frustrate layer sliding, and the presence of grain boundaries and interparticle strain would frustrate the shape change accompanying each grain's orthorhombic-to-monoclinic transition.

The different transitions in powders and single crystals highlights the importance of sample-dependent factors, but even nominally similar crystals can exhibit different behaviors, such as the broad transition seen in certain  $\text{MoTe}_2$  crystals [13]. In fact, recently, another study reported an ambient-pressure  $T_d$ - $1T'$  transition in a  $\text{WTe}_2$  crystal at 613 K via resistivity measurements [29], and, in contrast to our data, a hysteresis was observed. (This study also reported a broad  $T_d$ - $1T'$  transition in  $\text{WTe}_2$  powder via synchrotron XRD between 598 and 673 K, roughly consistent with our findings [29].) Presumably, sample-dependent factors are responsible for the presence of a hysteresis in the data of Ref. [29] and not in ours; e.g., it is possible that Te vacancies from evaporation play a role, which would be a smaller effect for the thicker samples needed for neutron scattering than the thinner samples usable for resistance measurements. A better understanding of sample-dependent factors influencing the transition may help realize the potential of stacking changes to influence properties in quasi-two-dimensional materials.

#### IV. CONCLUSION

Using elastic neutron scattering on a single crystal and XRD on a powder sample of  $\text{WTe}_2$ , we observed a  $T_d$ - $1T'$  structural phase transition in the Weyl semimetal  $\text{WTe}_2$  at ambient pressure. In the crystal, the transition occurs at  $\sim 565$  K without hysteresis, but in the powder, the transition is broadened and incomplete up to 700 K. Our results place constraints on theories of the structural behavior of  $\text{Mo}_{1-x}\text{W}_x\text{Te}_2$ , which thus far have not predicted a transition in  $\text{WTe}_2$ .

#### ACKNOWLEDGMENTS

This work has been supported by the Department of Energy, Grant No. DE-FG02-01ER45927. A portion of this research used resources at the High Flux Isotope Reactor, which is a DOE Office of Science User Facility operated by Oak Ridge National Laboratory. We acknowledge utilization of the FEI Quanta LV200 Environmental Scanning Electron Microscope instrument within UVa's Nanoscale Materials Characterization Facility (NMCF), as well as the assistance of Richard White for equipment training and analysis of the data.

- [1] K. Deng, G. Wan, P. Deng, K. Zhang, S. Ding, E. Wang, M. Yan, H. Huang, H. Zhang, Z. Xu, J. Denlinger, A. Fedorov, H. Yang, W. Duan, H. Yao, Y. Wu, S. Fan, H. Zhang, X. Chen, and S. Zhou, Experimental observation of topological Fermi arcs in type-II Weyl semimetal MoTe<sub>2</sub>, *Nat. Phys.* **12**, 1105 (2016).
- [2] Y. Wu, D. Mou, N. H. Jo, K. Sun, L. Huang, S. L. Budko, P. C. Canfield, and A. Kaminski, Observation of Fermi arcs in the type-II Weyl semimetal candidate WTe<sub>2</sub>, *Phys. Rev. B* **94**, 121113(R) (2016).
- [3] J. Yang, J. Colen, J. Liu, M. C. Nguyen, G. W. Chern, and D. Louca, Elastic and electronic tuning of magnetoresistance in MoTe<sub>2</sub>, *Sci. Adv.* **3**, eaao4949 (2017).
- [4] M. N. Ali, J. Xiong, S. Flynn, J. Tao, Q. D. Gibson, L. M. Schoop, T. Liang, N. Haldolaarachchige, M. Hirschberger, N. P. Ong, and R. J. Cava, Large, non-saturating magnetoresistance in WTe<sub>2</sub>, *Nature (London)* **514**, 205 (2014).
- [5] P. L. Cai, J. Hu, L. P. He, J. Pan, X. C. Hong, Z. Zhang, J. Zhang, J. Wei, Z. Q. Mao, and S. Y. Li, Drastic Pressure Effect on the Extremely Large Magnetoresistance in WTe<sub>2</sub>: Quantum Oscillation Study, *Phys. Rev. Lett.* **115**, 057202 (2015).
- [6] R. Clarke, E. Marseglia, and H. P. Hughes, A low-temperature structural phase transition in  $\beta$ -MoTe<sub>2</sub>, *Philos. Mag. B* **38**, 121 (1978).
- [7] B. E. Brown, The crystal structures of WTe<sub>2</sub> and high-temperature MoTe<sub>2</sub>, *Acta Cryst.* **20**, 268 (1966).
- [8] H. J. Kim, S. H. Kang, I. Hamada, and Y. W. Son, Origins of the structural phase transitions in MoTe<sub>2</sub> and WTe<sub>2</sub>, *Phys. Rev. B* **95**, 180101(R) (2017).
- [9] Y. Zhou, X. Chen, N. Li, R. Zhang, X. Wang, C. An, Y. Zhou, X. Pan, F. Song, B. Wang, W. Yang, Z. Yang, and Y. Zhang, Pressure-induced T<sub>d</sub> to 1T' structural phase transition in WTe<sub>2</sub>, *AIP Adv.* **6**, 075008 (2016).
- [10] J. A. Schneeloch, C. Duan, J. Yang, J. Liu, X. Wang, and D. Louca, Emergence of topologically protected states in the MoTe<sub>2</sub> Weyl semimetal with layer-stacking order, *Phys. Rev. B* **99**, 161105(R) (2019).
- [11] Y. Tao, J. A. Schneeloch, C. Duan, M. Matsuda, S. E. Dissanayake, A. A. Aczel, J. A. Fernandez-Baca, F. Ye, and D. Louca, Appearance of a T<sub>d</sub>\* phase across the T<sub>d</sub>-1T' phase boundary in the Weyl semimetal MoTe<sub>2</sub>, *Phys. Rev. B* **100**, 100101(R) (2019).
- [12] S. Dissanayake, C. Duan, J. Yang, J. Liu, M. Matsuda, C. Yue, J. A. Schneeloch, J. C. Y. Teo, and D. Louca, Electronic band tuning under pressure in MoTe<sub>2</sub> topological semimetal, *npj Quantum Mater.* **4**, 45 (2019).
- [13] J. A. Schneeloch, Yu Tao, C. Duan, M. Matsuda, A. A. Aczel, J. A. Fernandez-Baca, G. Xu, J. C. Neuefeind, J. Yang, and D. Louca, Evolution of the structural transition in Mo<sub>1-x</sub>W<sub>x</sub>Te<sub>2</sub>, *arXiv:2003.08531*.
- [14] X. J. Yan, Y. Y. Lv, L. Li, X. Li, S. H. Yao, Y. B. Chen, X. P. Liu, H. Lu, M. H. Lu, and Y. F. Chen, Composition dependent phase transition and its induced hysteretic effect in the thermal conductivity of W<sub>x</sub>Mo<sub>1-x</sub>Te<sub>2</sub>, *Appl. Phys. Lett.* **110**, 211904 (2017).
- [15] P. Lu, J. S. Kim, J. Yang, H. Gao, J. Wu, D. Shao, B. Li, D. Zhou, J. Sun, D. Akinwande, D. Xing, and J. F. Lin, Origin of superconductivity in the Weyl semimetal WTe<sub>2</sub> under pressure, *Phys. Rev. B* **94**, 224512 (2016).
- [16] J. Xia, D. F. Li, J. D. Zhou, P. Yu, J. H. Lin, J. L. Kuo, H. B. Li, Z. Liu, J. X. Yan, and Z. X. Shen, Pressure-induced phase transition in Weyl semimetallic WTe<sub>2</sub>, *Small* **13**, 1701887 (2017).
- [17] Y. Qi *et al.*, Superconductivity in Weyl semimetal candidate MoTe<sub>2</sub>, *Nat. Commun.* **7**, 11038 (2016).
- [18] C. Heikes, I. Lin Liu, T. Metz, C. Eckberg, P. Neves, Y. Wu, L. Hung, P. Piccoli, H. Cao, J. Leao, J. Paglione, T. Yildirim, N. P. Butch, and W. Ratcliff, Mechanical control of crystal symmetry and superconductivity in Weyl semimetal MoTe<sub>2</sub>, *Phys. Rev. Mater.* **2**, 074202 (2018).
- [19] S. M. Oliver, R. Beams, S. Krylyuk, I. Kalish, A. K. Singh, A. Bruma, T. Francesca, J. Joshi, I. R. Stone, S. J. Stranick, A. V. Davydov, and P. M. Vora, The structural phases and vibrational properties of Mo<sub>1-x</sub>W<sub>x</sub>Te<sub>2</sub> alloys, *2D Mater.* **4**, 045008 (2017).
- [20] Y. Y. Lv, L. Cao, X. Li, B. B. Zhang, K. Wang, B. Pang, L. Ma, D. Lin, S. H. Yao, J. Zhou, Y. B. Chen, S. T. Dong, W. Liu, M. H. Lu, Y. Chen, and Y. F. Chen, Composition and temperature-dependent phase transition in miscible Mo<sub>1-x</sub>W<sub>x</sub>Te<sub>2</sub> single crystals, *Sci. Rep.* **7**, 44587 (2017).
- [21] D. Rhodes *et al.*, Engineering the structural and electronic phases of MoTe<sub>2</sub> through W substitution, *Nano Lett.* **17**, 1616 (2017).
- [22] Y.-Y. Lv, B.-B. Zhang, X. Li, B. Pang, F. Zhang, D.-J. Lin, J. Zhou, S.-H. Yao, Y. B. Chen, S.-T. Zhang, M. Lu, Z. Liu, Y. Chen, and Y.-F. Chen, Dramatically decreased magnetoresistance in non-stoichiometric WTe<sub>2</sub> crystals, *Sci. Rep.* **6**, 26903 (2016).
- [23] B. H. Toby and R. B. Von Dreele, GSAS-II: The genesis of a modern open-source all purpose crystallography software package, *J. Appl. Cryst.* **46**, 544 (2013).
- [24] See Supplemental Material at <http://link.aps.org/supplemental/10.1103/PhysRevB.102.060103> for more details on the XRD refinement results.
- [25] S. Cho, S. H. Kang, H. S. Yu, H. W. Kim, W. Ko, S. W. Hwang, W. H. Han, D. H. Choe, Y. H. Jung, K. J. Chang, Y. H. Lee, H. Yang, and S. W. Kim, Te vacancy-driven superconductivity in orthorhombic molybdenum ditelluride, *2D Mater.* **4**, 021030 (2017).
- [26] R. He, S. Zhong, H. H. Kim, G. Ye, Z. Ye, L. Winford, D. McHaffie, I. Rilak, F. Chen, X. Luo, Y. Sun, and A. W. Tsen, Dimensionality-driven orthorhombic MoTe<sub>2</sub> at room temperature, *Phys. Rev. B* **97**, 041410(R) (2018).
- [27] S. Zhong, A. Tiwari, G. Nichols, F. Chen, X. Luo, Y. Sun, and A. W. Tsen, Origin of magnetoresistance suppression in thin  $\gamma$ -MoTe<sub>2</sub>, *Phys. Rev. B* **97**, 241409(R) (2018).
- [28] C. Cao, X. Liu, X. Ren, X. Zeng, K. Zhang, D. Sun, S. Zhou, Y. Wu, Y. Li, and J. H. Chen, Barkhausen effect in the first order structural phase transition in type-II Weyl semimetal MoTe<sub>2</sub>, *2D Mater.* **5**, 044003 (2018).
- [29] R. Dahal, L. Z. Deng, N. Poudel, M. Gooch, Z. Wu, H. C. Wu, H. D. Yang, C. K. Chang, and C. W. Chu, Tunable structural phase transition and superconductivity in the Weyl semimetal Mo<sub>1-x</sub>W<sub>x</sub>Te<sub>2</sub>, *Phys. Rev. B* **101**, 140505(R) (2020).